Evaluation and Intercomparison of Cloud Fraction and Radiative Fluxes in Recent Reanalyses over the Arctic Using BSRN Surface Observations

BEHNJAMIN J. ZIB, XIQUAN DONG, BAIKE XI, AND AARON KENNEDY

Department of Atmospheric Sciences, University of North Dakota, Grand Forks, North Dakota

(Manuscript received 10 March 2011, in final form 24 October 2011)

ABSTRACT

With continual advancements in data assimilation systems, new observing systems, and improvements in model parameterizations, several new atmospheric reanalysis datasets have recently become available. Before using these new reanalyses it is important to assess the strengths and underlying biases contained in each dataset. A study has been performed to evaluate and compare cloud fractions (CFs) and surface radiative fluxes in several of these latest reanalyses over the Arctic using 15 years (1994–2008) of high-quality Baseline Surface Radiation Network (BSRN) observations from Barrow (BAR) and Ny-Alesund (NYA) surface stations. The five reanalyses being evaluated in this study are (i) NASA's Modern-Era Retrospective analysis for Research and Applications (MERRA), (ii) NCEP's Climate Forecast System Reanalysis (CFSR), (iii) NOAA's Twentieth Century Reanalysis Project (20CR), (iv) ECMWF's Interim Reanalysis (ERA-I), and (v) NCEP–Department of Energy (DOE)'s Reanalysis II (R2). All of the reanalyses show considerable bias in reanalyzed CF during the year, especially in winter. The large CF biases have been reflected in the surface radiation fields, as monthly biases in shortwave (SW) and longwave (LW) fluxes are more than 90 (June) and 60 W m^{-2} (March), respectively, in some reanalyses. ERA-I and CFSR performed the best in reanalyzing surface downwelling fluxes with annual mean biases less than 4.7 (SW) and 3.4 W m^{-2} (LW) over both Arctic sites. Even when producing the observed CF, radiation flux errors were found to exist in the reanalyses suggesting that they may not always be dependent on CF errors but rather on variations of more complex cloud properties, water vapor content, or aerosol loading within the reanalyses.

1. Introduction

Over the past few decades, atmospheric reanalysis datasets have provided a long-term, gridded representation of the state of the atmosphere while offering a resource for investigating climate processes and predictability. Reanalyses utilize observations through state-of-the-art data assimilation systems. Combined with underlying models, they provide a continuous data record that consists of various atmospheric variables describing (diagnosing) past weather conditions. Reanalyses are used for a variety of applications, including as a source for the development and verification of climate models, forcing data for numerous user models, examining forecast skill, estimation of renewable energy resources, investigation of extreme weather and climatic events, and health risk assessments. These datasets may also be an essential tool for performing studies in data-sparse regions such as the Arctic. Given its unique environmental characteristics and extreme surface conditions, observations are often difficult to obtain and are thus limited in the polar regions. As the Arctic system continues to experience significant environmental changes at a greater rate than the rest of the world (Solomon et al. 2007; Serreze and Francis 2006), it has become an area of escalating attention and focus. While reanalyses offer a potential resource for the recognition and analysis of change in a sensitive and complex coupled Arctic climate system, the uncertainty in their reanalyzed variables must first be addressed.

Several studies have investigated the performance of reanalyses over the Arctic for a variety of fields including atmospheric moisture budgets (Bromwich et al. 2000, 2002), upper-level winds (Francis 2002), precipitation (Serreze and Hurst 2000), cloud fraction (CF) and radiative fluxes (Walsh et al. 2009), and general tropospheric

Corresponding author address: Dr. Xiquan Dong, Department of Atmospheric Sciences, University of North Dakota, 4149 University Ave. Stop 9006, Grand Forks, ND 58202-9006.
E-mail: dong@aero.und.edu

DOI: 10.1175/JCLI-D-11-00147.1

assessments (Bromwich and Wang 2005; Bromwich et al. 2007). These studies, however, were based on the earlier generations of reanalyses (e.g., Kalnay et al. 1996; Uppala et al. 2005; Onogi et al. 2007). With the recent advancements in data assimilation systems, changes in observing systems, and improvements in model parameterizations, several new reanalysis datasets have recently become available. Before using these new reanalyses it is important to assess the advantages and disadvantages of each reanalysis and identify the strengths and underlying biases associated with each dataset. Consequently, a study focused on the evaluation and intercomparison of five relatively new global reanalysis datasets has been conducted. The reanalyses being investigated are as follows: (i) the National Aeronautics and Space Administration (NASA)'s Modern-Era Retrospective; analysis for Research and Applications (MERRA) (Bosilovich et al. 2008; Rienecker et al. 2008); (ii) the National Centers for Environmental Prediction (NCEP)'s Climate Forecast System Reanalysis (CFSR) (Saha et al. 2010); (iii) National Oceanic and Atmospheric Administration (NOAA)'s Twentieth Century Reanalysis Project (20CR) (Compo et al. 2006, 2011; Whitaker and Hamill 2002); (iv) the European Centre for Medium-Range Weather Forecasts (ECMWF)'s Interim Reanalysis (ERA-I) (Dee and Uppala 2009; Simmons et al. 2007); and (v) NCEP–Department of Energy (DOE)'s reanalysis II (R2) (Kanamitsu et al. 2002). Unlike the other reanalyses, the NCEP–DOE R2 has been available for nearly a decade. It is important to note that it should not be considered a *next-generation* reanalysis, rather it is an update from the previous NCEP–National Center for Atmospheric Research (NCAR) reanalysis 1 (R1) (Kanamitsu et al. 2002). However, we have included R2 in this study to compare results with those found in a similar study by Walsh et al. (2009), which evaluated R1 and other earlier reanalyses. It is hoped that this study can objectively assess the strengths and weaknesses contained in each of these latest reanalyses and identify the areas of needed improvements for future reanalyses.

In this study, we have evaluated the accuracy of reanalyzed cloud fraction and downwelling surface radiation fluxes over the Arctic from the latest reanalyses using the Baseline Surface Radiation Network (BSRN) observations (Ohmura et al. 1998) during the period 1994–2008. BSRN offers high temporal resolution (1–3 min) solar and terrestrial radiation measurements from high accuracy instruments that provide a baseline for validating reanalyses and satellite estimates of surface radiation. The high-latitude BSRN sites used in this study are the NOAA's Barrow Observatory site in Barrow, Alaska (BAR), (71°19′N, 156°36′W) and Koldewey Station as part of the French–German Arctic Research Base at Ny-Alesund, Svalbard, Norway (NYA), (78°55′N, 11°56′E) (Fig. 1). BAR is located at the northernmost point in Alaska at roughly 8 m in altitude along the coast of the Beaufort Sea. NYA is located at the west coast of the island Spitsbergen in the Svalbard archipelago, one of the northernmost archipelagos in the Arctic. The surface type describing both high-latitude stations is tundra. While the topography at the BAR site is flat, the station at NYA is roughly 11 m in altitude and positioned in a mountain valley. These two BSRN sites were chosen for this study because they provide a long-term (over 15 years) data record, unlike many other sites across the Arctic.

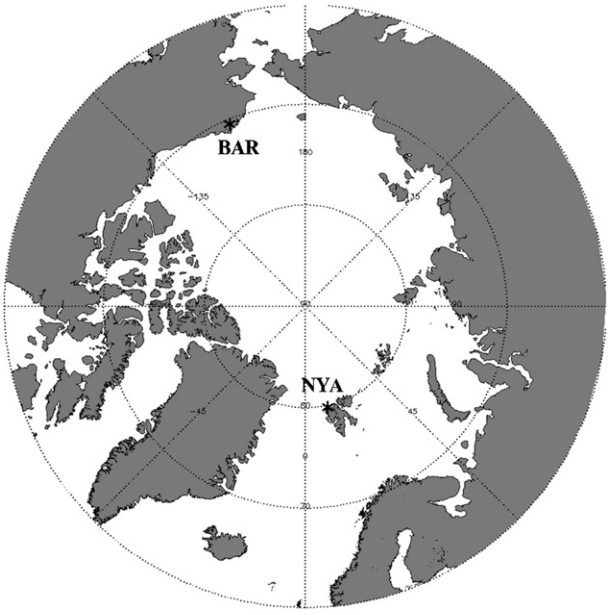

FIG. 1. Locations of BSRN high-latitude Arctic sites are shown: BAR (71°19′N, 156°36′W) and NYA (78°55′N, 11°56′E).

To determine in which season's biases are most pronounced, monthly mean biases in cloud fractions and surface radiation fluxes have been performed for each reanalysis. Root-mean-square errors (RMSEs) based on direct comparisons of 6-h means are also determined for each month to indicate the precision of each reanalysis compared to observations. While significant biases and considerable differences are likely to arise between these new reanalyses, it is expected that the majority should demonstrate better skill in capturing the observed surface radiation fluxes than the earlier reanalyses seen in Walsh et al. (2009).

2. Datasets and methodology

a. BSRN and ARM observations

The variables explored in this study are total CF, surface downwelling shortwave (SW-down) and longwave

(LW-down) radiation fluxes, and 2-m air temperatures. The broadband SW-down (0.3–3 μm) and LW-down (4–50 μm) fluxes at BAR were obtained by Eppley Precision Spectral Pyranometers (PSPs) and Precision Infrared Pyrgeometers (PIRs), respectively. Kipp and Zonen radiometers for SW radiation and Eppley PIRs for LW measurements were used at NYA. Observed surface radiation fluxes were available at a temporal resolution of 1–3 min. To avoid the temporal sampling biases in calculating monthly means, the SW and LW fluxes were first binned and averaged to 1-h and then to 6-h intervals. Because of the sinusoidal nature of radiative fluxes, this technique avoided biases owing to more or less samples occurring during individual hours within a 6-h period. Any 1-h period completely missing data resulted in the 6-h mean being omitted for this study. The 6-h averages were then used to directly compare with reanalyses and also to compute monthly and annual means during the 15-yr period.

At the BAR site, cloud fraction was derived from the Vaisala laser ceilometer located at the Atmospheric Radiation Measurement (ARM) North Slope of Alaska (NSA) (Ackerman and Stokes 2003) site (~1 km from the BAR site). The laser ceilometer is a self-contained, ground-based, and active (905 nm) remote sensing instrument designed to measure cloud-base height (up to 7.6 km) and potential backscatter signals by aerosols (Flynn 2004). Because of the limited measuring range of the ceilometer, some high clouds are expected to be missed. Dong et al. (2010) determined that annual CFs over BAR derived from ceilometer measurements were 3% lower than those derived from radar–lidar measurements as a result of missed high clouds (>7.6 km). One-hour cloud fraction over BAR is defined in this study as the percentage of cloudy returns within a 1-h sampling period. The hourly CFs were then averaged into 6-h means and monthly means. Monthly mean CF over NYA was obtained via human observations taken daily at 0600, 1200, and 1800 UTC. Monthly means of CF from both Arctic sites are based on 10 years of observations (1999–2008). More detailed information on BSRN data and instrument uncertainties can be found in the studies of Lanconelli et al. (2011), Ohmura et al. (1998), and Marty et al. (2003).

b. Atmospheric reanalyses

The variables analyzed in each of the reanalyses (MERRA, CFSR, R2, 20CR, and ERA-I) are made available at a variety of spatial and temporal resolutions (Table 1). Output from each reanalysis was temporally averaged into 6-h means for a consistent comparison between observations and reanalyses. Monthly mean biases and RMSEs in all of the reanalyses were calculated

TABLE 1. Reanalysis' spatial and temporal resolutions and corresponding distance from each station (BAR and NYA) location to the center of the closest grid point used in each reanalysis.

	MERRA		CFSR		R2		20CR		ERA-I	
	BAR	NYA	BAR	NYA	BAR	NYA	BAR	NYA	BAR	NYA
Distance from station (km)	19.75	8.39	3.11	9.76	33.66	19.83	33.66	19.83	78.07	63.82
Horizontal resolution	Global Gaussian grid (540 × 361) 0.66° × 0.5°		Global Gaussian grid (1152 × 576) 0.31° × 0.31°		Global Gaussian grid (192 × 94) 1.875° × 1.9°		Global Gaussian grid (192 × 94) 1.875° × 1.9°		Global Gaussian grid (240 × 121) 1.5° × 1.5°	
Vertical resolution	72 levels (to 0.01 hPa)		64 levels (to 0.26 hPa)		28 levels		28 levels		60 levels (to 0.1 hPa)	
Temporal resolution	1-h time avg		1-h time avg		6-h time avg		3-h time avg		6-h time avg.	
Approximate gridcell area (km^2)	1265	770	385	230	14 010	8360	14 010	8360	8820	5760

by using the closest grid point to the BSRN surface sites, except for ERA-I because of the distant location of this point to the surface sites. These distances (reanalysis nearest gridpoint location − station location) for each reanalysis are also listed in Table 1. Because of the gradients in CF and downwelling surface radiation fluxes that are present across the coastal regions in the Arctic, the four nearest grid points in the ERA-I were linearly interpolated for a more realistic interpretation of radiation fluxes and cloud fraction fields. This technique resulted in smaller errors than by using any of the nearest grid points for this reanalysis.

1) MERRA REANALYSIS

NASA's MERRA dataset is based on the Goddard Earth Observing System (GEOS) data Analysis System version 5 (GEOS-5 DAS; Bosilovich et al. 2008). GEOS-5 includes the GEOS-5 atmospheric general circulation model (AGCM) and the Gridpoint Statistical Interpolation (GSI) atmospheric analysis developed jointly with NOAA/NCEP/ Environmental Modeling Center (EMC). Also incorporated into GEOS-5 is incremental analysis updates (Bloom et al. 1996) to slowly adjust the model states toward the observed state. This global reanalysis takes advantage of a variety of recent satellite observations, such as NASA's Earth Observing System with a focus on improving estimates of the earth's hydrological cycle. The SW and LW radiation parameterizations used in MERRA are documented in Chou and Suarez (1999) and Chou et al. (2001), respectively. MERRA utilizes a prognostic cloud scheme in which clouds are assumed to be maximum–random overlapped.

2) R2 REANALYSIS

NCEP's R2 is an improved version of R1 that features updated parameterizations of physical processes while eliminating several previous errors (Kanamitsu et al. 2002). R2 uses an updated forecast model and data assimilation system along with improved diagnostic outputs and fixed fields from its predecessor R1. Relevant improvements to the model physics consist of a new SW radiation scheme (Chou 1992; Chou and Lee 1996) to remove excess surface insolation found in R1, updated cloud-tuning coefficients for stratus clouds, and radiation calculations performed on a full Gaussian grid at every hour as opposed to every 3 h in R1. Cloud fraction in R2 is diagnosed from an empirical relative humidity–cloud cover relationship and is assumed to be random overlapped (Xu and Randall, 1996). A more accurate system description and evaluation of R2 is documented in Kanamitsu et al. (2002).

3) 20CR REANALYSIS

NOAA's 20CR dataset uses a new version of the NCEP atmosphere–land model along with an Ensemble Kalman Filter data assimilation technique (Whitaker and Hamill 2002) that assimilates only surface pressure reports and observations while using observed the Hadley Centre Sea Ice and SST dataset (HadISST) sea surface temperatures and sea ice concentration fields (Rayner et al. 2003) for prescribed boundary conditions (Compo et al. 2011). As a result, a global analysis of the atmospheric state along with an uncertainty estimate is produced, which covers the entire twentieth century (1871–present). Such a long-term dataset can be advantageous in understanding the full range of variability in climate processes and extreme events while also providing significant information on long-term climate trends. The coupled atmosphere–land model uses an experimental version of the NCEP Global Forecast System (GFS) that includes an updated prognostic cloud condensate scheme (Moorthi et al. 2001), revisions to the solar radiative transfer model (Hou et al. 2002), and a Rapid Radiative Transfer Model (RRTM) developed at Atmospheric and Environmental Research for longwave radiative transfer (Mlawer et al. 1997). Cloud liquid water is a prognostic quantity from which cloud fraction is diagnosed. Clouds are also assumed to be maximum–random overlapped. More information about the 20CR system is documented in Compo et al. (2011).

4) CFSR REANALYSIS

NCEP's CFSR dataset is a global, high-resolution coupled atmosphere–ocean–land surface–sea ice model that was recently completed over the 31-yr period from 1979 to 2009. This reanalysis intends to provide initial conditions for historical forecasts and address calibration applications for the operational NCEP climate forecasts while also helping to provide accurate estimates of the earth's climate state over the satellite era. Atmospheric observations are assimilated via the three-dimensional variational (3DVAR) GSI system. CFSR implements the Operational Global Forecast System (atmospheric model), the new Modular Ocean Model version 4 (MOM4), the Operational Noah Land Model, and a new sea ice model. The primary novelties of the CFSR are (i) coupling of atmosphere and ocean during the generation of the 6-h guess field, (ii) an interactive sea ice model, and (iii) assimilation of satellite radiances by GSI. Standing out from the earlier reanalyses, CFSR operates at a much higher spatial (T382, ~38 km) and temporal (one hour) resolution. The CFSR utilizes a RRTM for shortwave (Iacono et al. 2000; Clough et al. 2005) and infrared (Mlawer et al. 1997) radiation with

maximum–random cloud overlap and a prognostic cloud condensate from which cloud cover is diagnosed (Saha et al. 2006). A more detailed description of the CFSR system and model components is documented in Saha et al. (2006) along with supplemental material (Saha et al. 2010).

5) ERA-INTERIM REANALYSIS

The ERA-I is the latest ECMWF reanalysis that covers the period from 1989 to the present. It was created in preparation for the next-generation extended reanalysis to replace the former 40-yr ECMWF (ERA-40) reanalysis. The ERA-Interim atmospheric model and reanalysis system uses cycle 31r2 of ECMWF's Integrated Forecast System (IFS) (Berrisford et al. 2009). This atmospheric model is coupled to an ocean–wave model. Several differences were made in data assimilation and observations between the ERA-I and ERA-40 reanalysis. Some of these advances in ERA-I include the use of 12-h 4DVAR, a T255 horizontal resolution, improved model physics, and an improved fast radiative transfer model. ERA-I also utilizes the RRTM for the longwave radiation transfer scheme (Mlawer et al. 1997). A prognostic cloud scheme is implemented in ERA-I in which clouds are assumed to be maximum–random overlapped. Further details on ERA-I analysis system and performance can be found in documentation (Berrisford et al. 2009) and are described in numerous ECMWF newsletters.

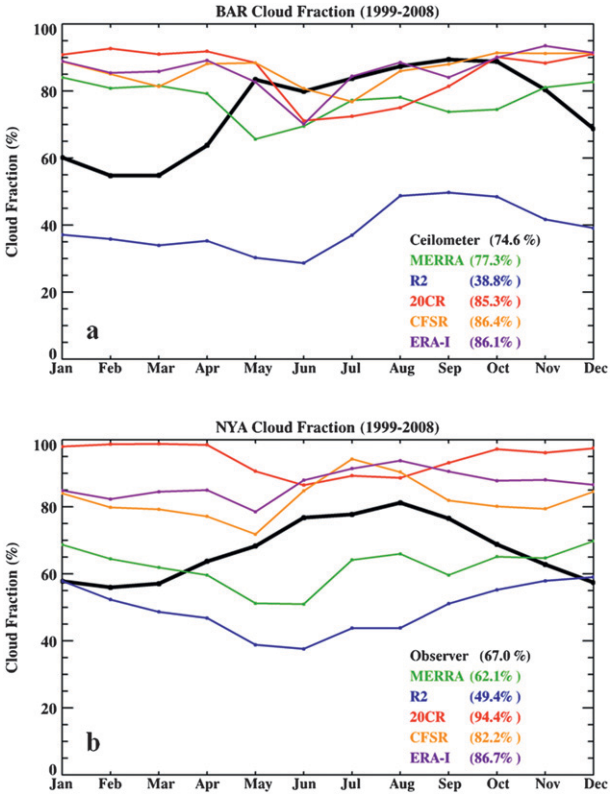

FIG. 2. Monthly mean total cloud fractions reanalyzed from MERRA (green), CFSR (orange), R2 (blue), 20CR (red), and ERA-I (purple) compared with observations (black) at (a) BAR and (b) NYA during the period 1999–2008. Values in parenthesis indicate corresponding annual mean CFs.

3. Results and discussion

Comparisons of CF, 2-m air temperature, and SW-down and LW-down surface fluxes in recent reanalyses with BSRN observations have been performed over two Arctic locations: BAR and NYA. There are five subsections in this section; they are CF, SW-down, and LW-down comparisons between reanalyses and surface observations in sections 3a–c. Sections 3d–e examine the RMSEs and the relationships between the CF errors and radiation errors, respectively.

a. CF

As demonstrated in Fig. 2a, as well as in the Dong et al. (2010) study, the monthly mean CF from the ARM NSA ceilometer increases from March to May (55% → 83%), remains high from May to October (85%), and then decreases from November until the following March (80% → 55%). Four of the five reanalyses (MERRA, 20CR, CFSR, and ERA-I) have minimal seasonal variations in their reanalyzed CF. Although they are similar in magnitude to the observed CF from May to October, they have large positive biases (+15% → +40%) from November to the following April. Despite the improvements made to the cloud parameterizations from R1 to R2, R2 stands out with large negative biases year-round (−35.8%, annual mean) at BAR.

Observed and reanalyzed monthly mean CFs over NYA are illustrated in Fig. 2b. The observed CF increases from February (56%) until its peak in August (81%) before decreasing at a near constant rate until December (57%). CFSR and ERA-I capture this observed increase in CF during the late spring and summer, despite having positive biases throughout the year. Once again, R2 underestimates CF, with biases as low as −40% during the summer. During the cold season, four of the five reanalyses analyzed CFs much larger than those observed, suggesting a potential problem with the cloud parameterizations during winter. The largest biases during this time are seen in 20CR as reanalyzed CFs are on average 41% higher than those observed. It is important to note that the CF biases over NYA may be suspect because of the uncertainties arising from human observations, especially during the polar night. Hahn et al. (1995)

determined the human-observed cloud cover over the Arctic was reduced by up to 5% when inadequate moonlight was present. This may result in a negative bias in observed CF over NYA, especially during the long and continuous months of darkness. Regardless of these uncertainties in cloud detection, the large positive CF biases in the majority of the reanalyses during winter months illustrate reasons for concern regarding cloud parameterizations in these reanalyses.

For the annual average, CFs in MERRA agree best (+2.7% over BAR, −4.9% over NYA) with observations over the two Arctic sites, while those reanalyzed from R2 agree the least (−35.8% over BAR, −17.6% over NYA). The best agreement in CF throughout the reanalyses occurs during the warm season (May–October) with the exception of R2.

b. SW-down

Seasonal CF biases can have considerable effects on the radiation fields in each of the reanalyses. Surface radiation fluxes play a vital role in the Arctic climate system through snow/ice–albedo feedbacks (Curry et al. 1995), regulation of surface temperatures, and their influence on sea ice variability (Francis et al. 2005; Kay et al. 2008). Unlike most regions in the world, clouds have an overall annual net warming effect in polar regions as the LW warming effect becomes more dominant than the SW cooling effect (Dong et al. 2010).

Figure 3a illustrates the monthly mean observed and reanalyzed SW-down fluxes over BAR. The observed SW-down flux increases from winter to summer with a peak of 263 W m^{-2} in June. With a persistent negative bias in CF, R2 contains large positive biases in surface SW-down flux (up to +87 W m^{-2}) throughout the year. Compared to the observed SW-down flux, MERRA has a negative bias for most of the year (−9.7 W m^{-2}), with better agreement during late summer and fall. 20CR transitions from negative to positive biases in SW-down flux between May and June. This transition is coincident with the transition in CF biases in 20CR (Fig. 2a). Both CFSR and ERA-I reanalyzed SW-down fluxes agree very well with the observations throughout the entire year with annual mean biases of +2.6 and −2.1 W m^{-2}, respectively.

Generally, positive (negative) biases in surface SW-down fluxes are associated with negative (positive) biases in CF. This conclusion is supported by the negative biases in SW-down flux corresponding to positive biases in CF during March–April from four of the five reanalyses. This is also seen in 20CR as the positive (negative) biases in CF during March–May (June–September) correspond to negative (positive) biases in SW-down flux. This is not the case, however, for MERRA as both

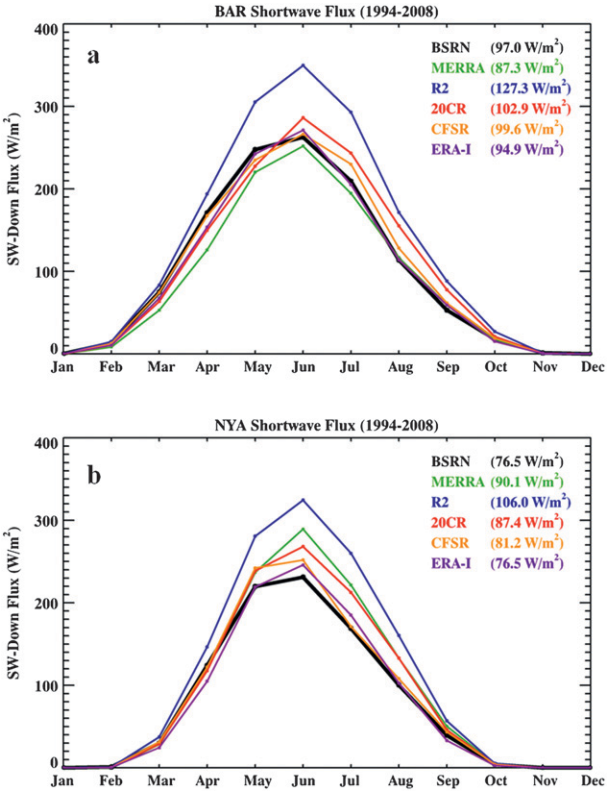

FIG. 3. Monthly mean SW-down fluxes reanalyzed from five reanalyses compared with BSRN observations (black) at (a) BAR and (b) NYA during the period 1994–2008. Values in parenthesis indicate corresponding annual mean fluxes.

CF and SW-down fluxes have negative biases during the period May–October. Other parameters, including cloud optical depth and cloud height, should be investigated in the future as they also play key roles in determining the SW-down flux (Dong and Mace 2003; Dong et al. 2010). Besides the cloud properties, the distribution of aerosol and other trace gases such as ozone and water vapor contained in the reanalyses can have a significant influence on the reanalyses' radiation parameterizations. Furthermore, the surface albedo can be an important factor in determining the amount of SW-down flux at the surface through its role in multiple reflections between the highly reflective surface and cloud (Wendler et al. 1981).

Figure 3b shows the observed and reanalyzed monthly mean SW-down fluxes over the NYA site. ERA-I monthly mean SW-down fluxes are nearly the same as those observed throughout the entire year, while other reanalyses contain annual biases from +4.7 W m^{-2} (CFSR) to +29.5 W m^{-2} (R2). Similar to the BAR comparisons, the reanalyses' monthly mean SW-down fluxes are much higher than those observed during summer and fall

TABLE 2. Monthly and seasonal biases of downwelling SW and LW fluxes over BAR and NYA for each reanalysis (W m^{-2}). Bold values represent the lowest biases.

	Shortwave downwelling flux bias											
	BAR						NYA					
	BSRN	MERRA	CFSR	R2	20CR	ERA-I	BSRN	MERRA	CFSR	R2	20CR	ERA-I
Jan	0.2	−0.2	−0.2	−0.2	−0.2	−0.1	0.0	0.0	0.0	0.0	0.0	0.0
Feb	13.1	−4.7	−0.5	+1.7	−2.6	−2.5	1.0	−0.6	−0.4	−0.3	−0.5	−0.5
Mar	74.9	−22.0	−0.4	+8.6	−11.4	−7.5	29.9	−1.5	+1.4	+7.5	−1.0	−5.4
Apr	171.1	−45.0	−3.5	+22.8	−21.2	−17.4	124.1	−6.3	−2.1	+22.5	−6.4	−19.2
May	247.7	−27.4	−12.7	+57.6	−20.1	−5.4	219.8	+17.3	+22.4	+61.0	+18.9	−0.6
Jun	262.6	−10.7	+3.7	+87.0	+23.6	+8.6	231.2	+58.2	+20.7	+93.4	+36.9	+14.7
Jul	209.3	−14.7	+20.5	+83.6	+34.0	−4.2	168.9	+52.6	+2.3	+91.0	+43.6	+16.1
Aug	113.8	+2.8	+14.4	+57.8	+41.3	+0.3	100.3	+32.5	+7.7	+60.0	+32.7	+2.4
Sep	53.0	+6.4	+8.5	+35.2	+24.7	+6.2	39.3	+11.0	+4.0	+17.5	+6.6	−6.3
Oct	17.7	−0.1	+1.2	+9.3	+3.2	−2.6	4.0	+0.2	+0.2	+1.0	+0.1	−1.4
Nov	1.2	−0.6	−0.4	−0.2	−0.4	−0.6	0.0	0.0	0.0	0.0	0.0	0.0
Dec	0.0	0.0	0.0	0.0	0.0	0.0	0.0	0.0	0.0	0.0	0.0	0.0
Dec–Feb (DJF)	4.5	−1.6	**−0.2**	+0.5	−0.9	−0.9	0.3	−0.2	−0.1	−0.1	−0.2	−0.2
Mar–May (MAM)	164.5	−31.4	**−5.6**	+29.7	−17.6	−10.1	124.6	**+3.2**	+7.2	+30.3	+3.8	−8.4
Jun–Aug (JJA)	195.2	−7.5	+12.9	+76.1	+33.0	**+1.6**	166.8	+47.8	**+10.2**	+81.5	+37.7	+11.1
Sep–Nov (SON)	24.0	+1.9	+3.1	+14.8	+9.1	**+1.0**	14.5	+3.7	+1.4	+6.2	+2.2	**−2.6**
ANNUAL	97.1	−9.7	+2.5	+30.3	+5.9	**−2.1**	76.5	+13.6	+4.7	+29.5	+10.9	**0.0**
	Longwave downwelling flux bias											
	BAR						NYA					
	BSRN	MERRA	CFSR	R2	20CR	ERA-I	BSRN	MERRA	CFSR	R2	20CR	ERA-I
Jan	182.8	+8.9	−1.4	−20.2	+52.9	−8.9	218.7	−17.3	+5.6	−14.1	+30.8	−4.7
Feb	179.2	+11.6	−0.4	−15.7	+58.3	−5.6	213.5	−16.3	+7.1	−13.0	+33.5	−4.4
Mar	176.1	+20.5	+3.3	−11.8	+61.0	−2.7	214.8	−18.7	+5.1	−14.0	+34.4	−3.1
Apr	212.7	+13.2	+6.2	−21.2	+42.3	+1.9	230.6	−19.8	+1.9	−18.9	+28.3	−0.5
May	260.8	−13.0	+6.6	−39.9	+15.5	−4.7	257.8	−27.7	−11.0	−30.5	+7.7	−4.2
Jun	286.9	−8.1	+5.0	−34.8	−0.4	+7.6	290.1	−34.8	−5.9	−38.8	−2.0	−3.3
Jul	303.8	−6.6	−4.8	−32.8	−5.9	+11.7	309.7	−25.6	+1.4	−38.0	−6.0	−1.3
Aug	311.5	−15.9	−6.3	−36.1	−16.0	+1.4	305.5	−26.4	−1.2	−36.5	−7.3	+1.6
Sep	297.2	−22.6	−4.0	−36.5	−16.5	−10.4	279.5	−27.9	−5.0	−22.3	+5.8	+6.5
Oct	261.0	−19.4	+1.7	−38.9	−3.0	−14.1	249.2	−22.6	−4.4	−15.0	+15.2	+1.8
Nov	220.5	−1.4	+5.4	−32.0	+19.6	−8.5	238.7	−24.2	−3.8	−16.3	+17.7	−2.3
Dec	192.9	+7.0	−0.4	−24.9	+44.5	−8.4	227.4	−18.2	+4.1	−14.1	+21.9	−1.8
DJF	185.0	+9.2	**−0.8**	−20.3	+51.9	−7.7	219.8	−17.3	+5.6	−13.7	+28.7	**−3.7**
MAM	216.5	+6.9	+5.4	−24.3	+39.6	**−1.8**	234.4	−22.1	**−1.4**	−21.1	+23.5	−2.6
JJA	300.7	−10.2	**−2.0**	−34.5	−7.5	+6.9	301.8	−28.9	−1.9	−37.8	−5.1	**−1.0**
SON	259.6	−14.5	+1.0	−35.8	**0.0**	−11.0	255.8	−24.9	−4.4	−17.9	+12.9	**2.0**
Annual	240.5	−2.2	**+0.9**	−28.7	+21.0	−3.4	252.9	−23.3	**−0.5**	−22.6	+15.0	−1.3

seasons. Unlike the BAR comparisons however, they agree well with observations during the spring. The largest positive biases in R2 and MERRA occur during summer months (+81.5 and +47.8 W m^{-2}, respectively) coinciding with their large negative CF biases. The monthly, seasonal, and annual biases in SW-down and LW-down flux from each reanalysis are listed in Table 2.

c. *LW-down*

In the absence of solar radiation during the polar winter, downwelling LW radiation flux plays a key role in determining the surface energy budget and influencing the overall state of the Arctic system. The observed monthly mean LW-down flux over the BAR site decreases from 180 to 170 W m^{-2} from January to March, increases from March to August (315 W m^{-2}), and finally decreases gradually into winter (Fig. 4a). While the positive LW-down bias in 20CR is coincident with its positive CF bias, an existing warm lower-tropospheric polar temperature bias in 20CR is likely a major contributor to this LW-down bias (Compo et al. 2011). This is a well-known and documented issue in 20CR and was found to arise from a misspecification of the sea ice

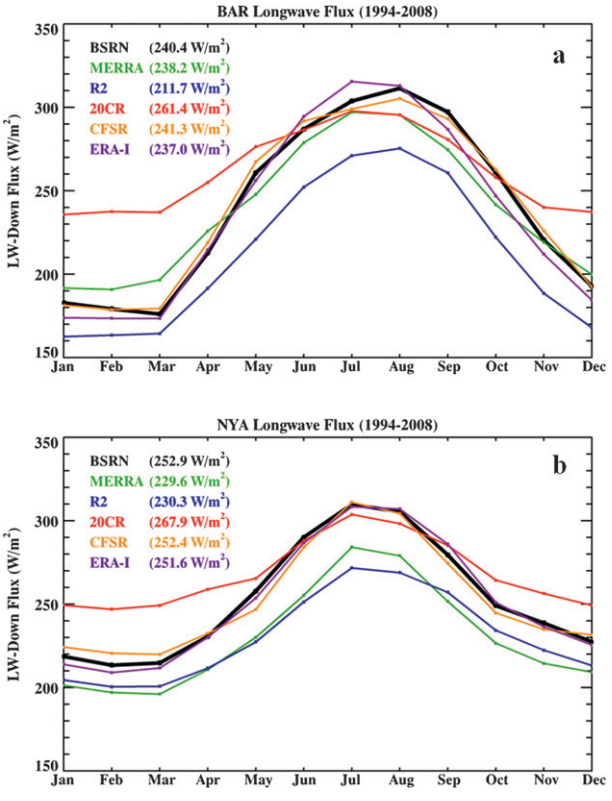

FIG. 4. As in Fig. 3, but for surface LW-down surface flux.

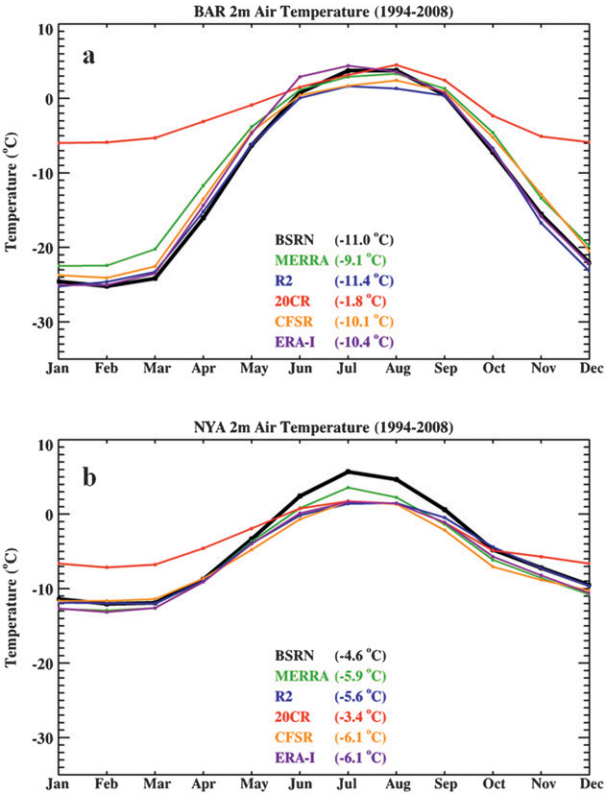

FIG. 5. Monthly mean 2-m air temperatures (°C) reanalyzed from five reanalyses compared with BSRN observations (black) at (a) BAR and (b) NYA during the period 1994–2008. Values in parenthesis indicate corresponding annual mean temperatures.

concentration along the coastal areas, which will be corrected in future versions of the reanalysis (Compo et al. 2011). As illustrated in Fig. 5a, wintertime 2-m air temperatures in 20CR are +18°C warmer than observations. Similar to their SW-down comparisons, the ERA-I and CFSR show the smallest annual mean biases (−3.4 and +0.9 W m^{-2}, respectively) as they capture the overall shape and amplitude of the observed annual cycle of LW-down fluxes. Interestingly, MERRA, 20CR, and ERA-I reanalyses illustrate a premature peak in LW-down flux during July, one month earlier than the observed peak in August.

Although the seasonal variation of LW-down fluxes over NYA is similar to that over BAR, its annual mean flux (253 W m^{-2}) is larger and peaks one month earlier in July. Despite the fact that NYA is located at higher latitude than BAR, its wintertime temperatures are much warmer. Relative to its latitudinal location, NYA has a rather mild climate as a result of warm waters from the Gulf Stream flowing northward along the west coast of the island. For example, air temperatures in February are 13°C warmer at NYA than those at BAR (Figs. 5a,b). Besides the warmer air temperatures, spatial differences in water vapor content between BAR and NYA may also play a role in increasing LW-down fluxes. In location with the North Atlantic cyclone track, water vapor over NYA is relatively abundant (Serreze et al. 1995). Together, the warmer temperatures and abundance of water vapor may explain the higher values observed in LW-down flux over NYA relative to BAR during the wintertime.

While the LW-down fluxes from ERA-I, 20CR, and MERRA reanalyses peaked one month earlier than observations over BAR, all of the reanalyses capture the observed peak in July over NYA (Fig. 4b). The effects of the noted warm temperature bias and positive CF bias during the cold season are shown in the LW-down fluxes in 20CR, where wintertime biases reach +29 W m^{-2} and springtime biases reach +24 W m^{-2} over NYA. MERRA, despite having the least biases in 2-m air temperature during summer (Fig. 5b), along with R2 shows the largest negative biases throughout the year with annual mean biases of −23.3 and −22.6 W m^{-2}, respectively. These are consistent with their negative CF biases. Similar to its results over BAR, the CFSR and ERA-I reanalyzed LW-down fluxes agree very well with observations over NYA, containing annual mean biases of −0.5 and −1.3 W m^{-2}, respectively.

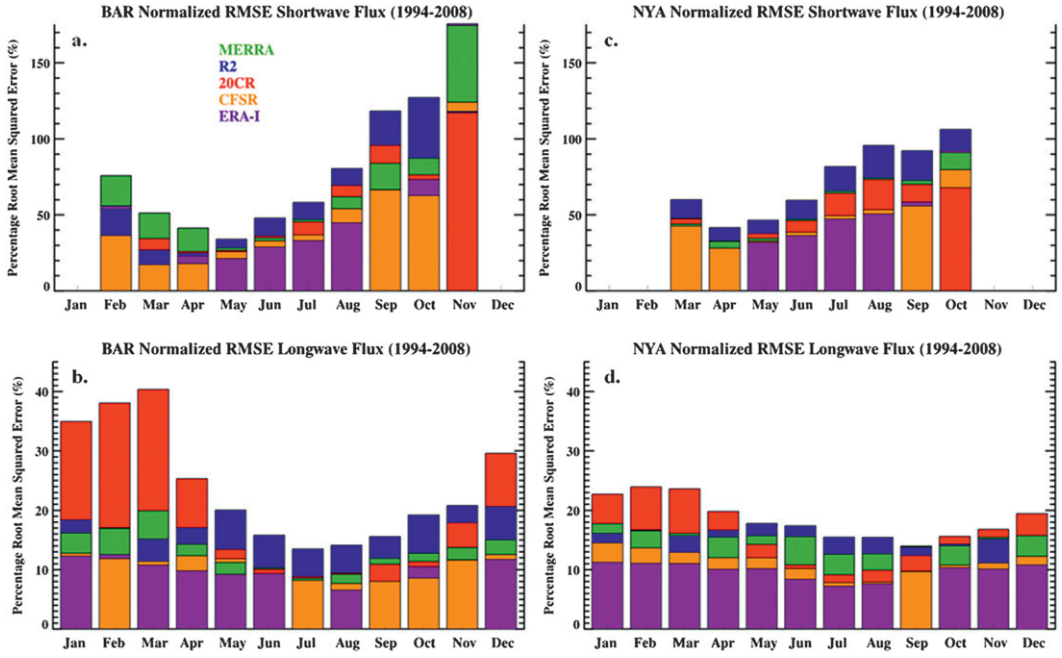

FIG. 6. Monthly RMSEs in (a) SW-down and (b) LW-down fluxes over BAR. (c),(d) As in (a),(b), but over NYA site. All reanalyses start at zero on *y* axis. Values are based on 6-h means during the 15-yr period (1994–2008). RMSEs are normalized by the observed mean flux for each month and are represented as a percentage.

In some cases, the LW-down biases cannot be explained by the CFs. For example, wintertime CFs over BAR in MERRA, ERA-I, and CFSR are much higher than what was observed, whereas their LW-down fluxes during this time period closely match observations, indicating that other parameters in these three reanalyses may play key roles in determining the LW-down fluxes. As demonstrated in the studies of Dong et al. (2006, 2010), all-sky LW-down fluxes are strongly influenced by variations in not only in CF but also cloud-base temperatures, cloud heights, and cloud liquid water path. For instance, high clouds, such as cirrus clouds, are very effective at trapping longwave radiation and emitting it back down to the earth's surface. Examining the reanalyzed cloud amounts at various altitudes along with their physical properties may be beneficial in helping explain the LW-down errors in the reanalyses and should be investigated in future studies.

d. RMSEs

Although monthly mean biases offer guidance about the performance of these reanalyses, they do not tell the whole picture as low biases can result from the cancellation of positive and negative errors. RMSEs can account for this issue and provide additional information about the precision of each reanalysis with observations.

Figures 6a and 6c illustrate the monthly RMSEs in SW-down flux over BAR and NYA, respectively. RMSEs were normalized for each month by the observed monthly mean flux and are represented as a percentage. ERA-I has the smallest RMSEs during May–August, while CFSR has the smallest RMSEs during the other months over the two surface sites. Over BAR, MERRA has the largest RMSEs during the first few months of daylight, while R2 has the largest RMSEs during the summer and autumn months, exceeding 110% during October. The largest RMSEs over BAR are seen in November when only a couple weeks of sunlight are present. Further investigation found that an early onset (1–2 days) of total darkness (polar nighttime) in the reanalyses compared with observations is responsible for the large RMSE percentages in November. Over NYA, R2 shows the largest RMSEs in every month. At both Arctic sites, the smallest RMSEs in all of the reanalyses occur during the middle of spring.

Similar results appear in the LW-down RMSEs (Figs. 6b,d) as CFSR and ERA-I have the smallest RMSEs throughout the year over both BAR and NYA. As expected, 20CR is responsible for the largest RMSE (up to 41%) during the winter and early spring seasons. During the summertime and early autumn, R2 shows the largest RMSE ranging from 14% to 21% over both stations.

e. Relationship between CF and radiative flux errors

To determine whether the radiative flux biases resulted from CF errors or other parameterization issues

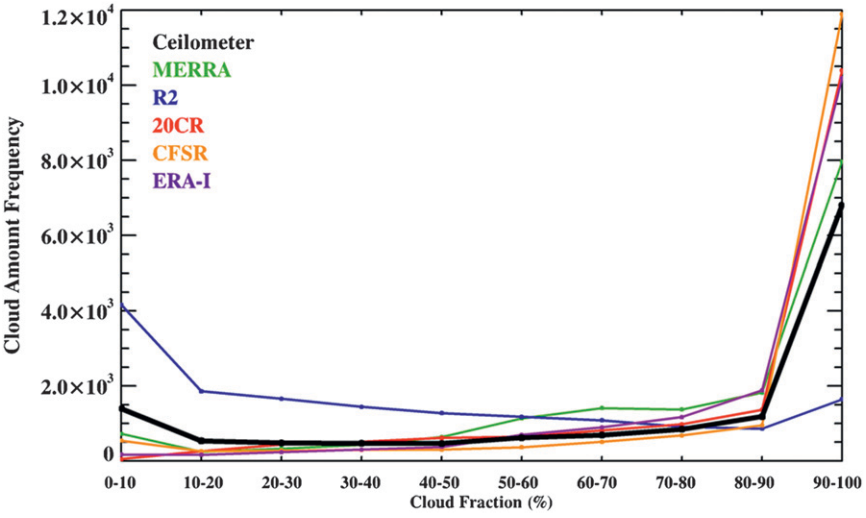

FIG. 7. Frequency of all available 6-h mean cloud fractions over BAR from January 1998 to December 2008. Cloud fractions were binned by every 10%.

within the reanalyses, clear-sky scenes were investigated. Figure 7 illustrates the cloud amount frequencies for all 6-h mean samples over BAR from January 1998 to December 2008. All of the reanalyses except for R2 have limited clear-sky samples. As a result, matching clear-sky scenes between reanalyses and observations is difficult. The amount of observed CF samples increased significantly (4 ~ 5 times) in the 90%–100% CF bin and even more in the reanalyses, with the exception of R2.

To further investigate how the frequency and distribution of CF errors in the reanalyses impact the radiative flux biases, consider Figs. 8 and 9. The abscissa in Figs. 8 and 9 represents the CF difference (reanalysis − observation) with a bin width of 5% CF, and the ordinate represents the frequency of occurrence for each CF difference (ΔCF) based on 11 years (1998–2008) of 6-h mean comparisons over BAR. The 0% ΔCF bin represents the samples when both reanalysis and observation have the same CF, while the positive and negative ΔCF bins represent the overestimate and underestimate from the reanalysis, respectively. Shaded within each ΔCF bin is the associated mean SW flux differences (Fig. 8) and LW flux differences (Fig. 9) (reanalysis − observation). The left column in each figure is the ΔCF and flux differences during the months of February and March, and the right column is the differences during June and July. June and July were chosen to represent the warm season because some of the largest biases in SW-down flux occurred in these months. February and March were chosen to represent the cold season when enough daylight was present to investigate SW-down flux differences. Also the largest biases in CF were observed in these months.

1) FREQUENCY AND DISTRIBUTION OF CLOUD FRACTION DIFFERENCES

The 0% ΔCF bin is the most frequent during June and July in the majority of the reanalyses, especially CFSR where 26% of all reanalyzed 6-h mean CFs match observations (Fig. 8, right column). The frequency distributions of ΔCFs within these reanalyses appear normal, with the exception of R2. This demonstrates that during the summer months (June–July) the amount of negative CF errors and positive CF errors are nearly equal. On the other hand, R2 illustrates a skewed and one-sided distribution that monotonically increases with larger negative ΔCFs, indicating a persistent underestimation during summer.

There is a noticeable change in the overall distribution of ΔCFs between the cold season (left column) and the warm season (right column). Unlike the summer months, the frequency distributions of ΔCFs for February and March are more one sided and bimodal as four of the five reanalyses have peaks in both 0% and +100% ΔCF bins. The latter peak (+100% ΔCF) indicates that the reanalyses often estimate 100% CF when clear skies are actually observed. The one-sided distributions in these four reanalyses demonstrate that they produce too many clouds during February and March. R2 on the other hand, continues to show more frequent negative ΔCFs, indicating a persistent underestimation of CF. Examining the frequency distributions of ΔCFs during different seasons provides a more in-depth assessment of the CF biases contained in the reanalyses and may offer guidance on needed improvements in the models' cloud parameterizations during different seasons.

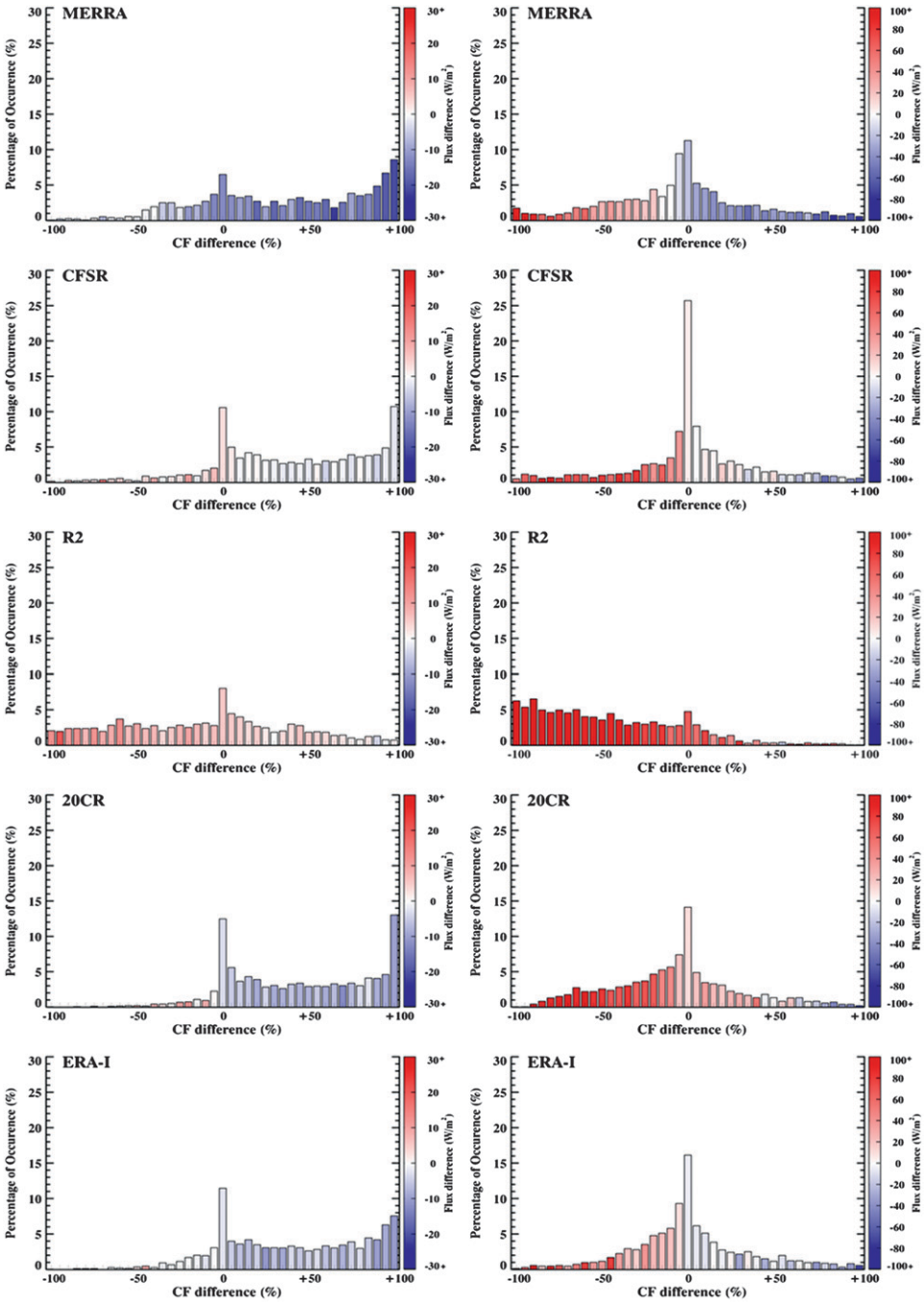

FIG. 8. Frequency distributions of CF differences (reanalysis − observation) for (left) February–March and (right) June–July over BAR. Shaded within each 5% ΔCF bin is the associated SW-flux differences (reanalysis − observation) for each dataset. The red colors represent the overestimated radiative flux from reanalysis, while the blue color is the underestimated flux. Ordinate is percentage of occurrence for each ΔCF bin and based on 11 years (1998–2008) of 6-h mean samples.

2) SURFACE RADIATIVE FLUX DIFFERENCES

Shaded within each ΔCF bin is the associated mean SW (Fig. 8) and LW (Fig. 9) flux differences (reanalysis − observations). Negative (positive) LW differences should be associated with negative (positive) CF differences, while the opposite is true for SW differences. As illustrated in Fig. 9, this is true, except in R2.

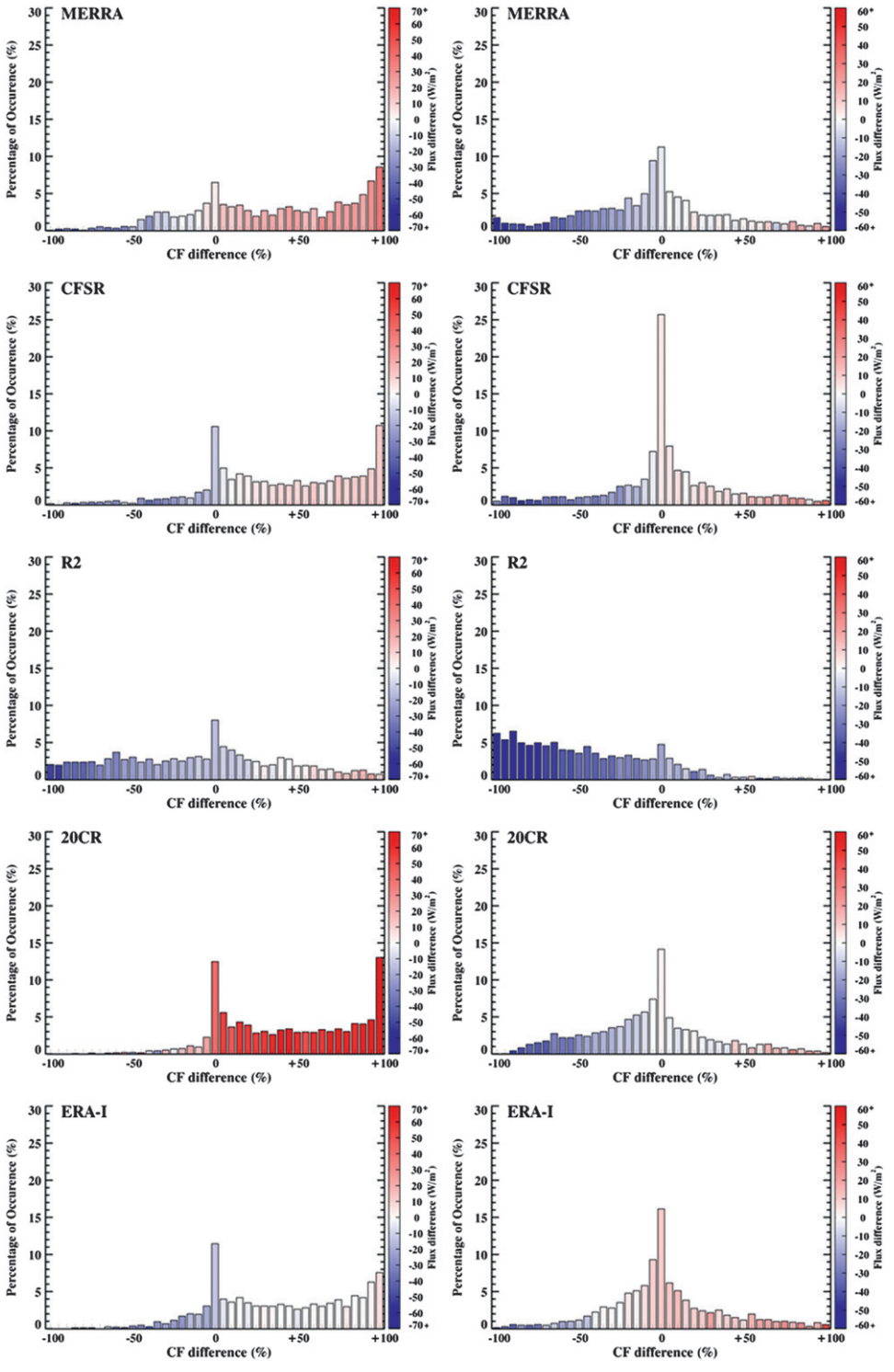

FIG. 9. As in Fig. 8, but for LW-flux differences.

The most informative part of Fig. 9 is the 0% ΔCF bin. Since this bin is the most frequently populated, the radiation flux differences associated with this bin are the most influential on the overall flux bias. A good example to demonstrate this is illustrated in the left column of Fig. 9 where the CFSR has positive LW-down flux differences (red) associated with positive ΔCFs the majority of time. However, when CFSR accurately analyzes

CFs (0% ΔCF bin), it contains negative flux differences (blue) that balance out the overall flux bias. This conclusion is shown in Fig. 4 during February–March as LW flux biases are nearly zero in CFSR.

Another important aspect of the 0% ΔCF bin is the fact that it removes the influence of clouds errors on radiative flux errors. Therefore, the flux differences associated with the 0% ΔCF bin provide insight into the possible radiation parameterization issues within the reanalyses. For example, SW flux differences in MERRA (R2) are still negative (positive) in the 0% ΔCF bin during both seasons (Fig. 8). Also, in 20CR when ΔCFs are zero, negative flux differences still exist during the cold season and positive flux differences are present during the warm season. Similarly, the majority of the reanalyses show LW-down flux differences despite correctly estimating the observed CF (Fig. 9). This suggests that the radiative flux biases in certain reanalyses may not always be dependent on CF biases but rather on variations of more complex cloud properties (cloud optical depth, cloud-base temperatures, and cloud type), water vapor content, and even aerosol loading profiles within the reanalyses. An investigation of these variables may lead to a better understanding of their effects and interactions with radiative fluxes within the reanalyses.

4. Summary and conclusions

In this study, we perform an evaluation and intercomparison of CF and surface radiative fluxes reanalyzed in five recent reanalyses utilizing BSRN observations during the period 1994–2008 over two Arctic sites: Barrow (BAR) and Ny-Alesund (NYA). This evaluation and intercomparison provides a quantitative estimate of the uncertainties or biases in CF and surface SW- and LW-down fluxes from these reanalyses over the Arctic region. Based on the 15-yr comparisons between reanalyses and observations, we reached the following conclusions.

1) The majority of the reanalyses illustrate difficulties in capturing the observed CFs during the wintertime with positive biases as large as +41% (20CR). Reanalyzed CFs in all of the reanalyses, except R2, agree better with observations during the warm season (May–October). On the annual average, the CFs in MERRA agree best with the observed CFs over two Arctic sites, while those in R2 agree the least.
2) Both CFSR and ERA-I contained the lowest biases in annual mean SW-down fluxes (less than 4.7 W m^{-2}), the lowest RMSEs and highest correlations over both Arctic sites compared to observations. On the contrary, R2 illustrates large positive biases in surface SW-down flux (up to +87 W m^{-2}) throughout the year in association with a persistent underestimation in CF.
3) The LW-down flux comparisons between observations and reanalyses are strongly related to their CF comparisons. The CFSR and ERA-I reanalyses again performed the best with an annual mean agreement within 3.4 W m^{-2} to observations. Over both Arctic sites, 20CR contained large positive biases in LW-down flux during the winter (up to +51.9 W m^{-2}) in association with a cloudy (up to +41%) and warm temperature (up to +18°C) bias. Over NYA, MERRA, and R2 contained the largest negative biases throughout the year with annual mean biases of −23.3 and −22.6 W m^{-2}, respectively.
4) During the summer, the majority of the reanalyses illustrate a normal frequency distribution in CF differences with a peak in the 0% ΔCF bin. During the cold season, the reanalyses encompass a one-sided and bimodal distribution in the frequency of CF differences with peaks at both 0% and +100% ΔCF, indicating that the reanalyses generally overestimate CF during the cold season. Also, in several reanalyses, SW and LW flux differences were found to exist despite correctly analyzing the observed CF. This suggests that the radiative flux biases may not always be dependent on CF errors but rather on variations of more complex cloud properties, along with aerosol and trace gas loading profiles.

Overall, ERA-I and CFSR were the best performers in this study for both Arctic sites. Surface radiative fluxes were very well reanalyzed in both these reanalyses as compared with observations. MERRA's performance was overall in the middle as it often fell between the reanalyses with the lowest bias and RMSE's (CFSR and ERA-I) and the ones with the largest (R2 and 20CR) in surface downwelling radiative fluxes. NCEP R2 continued to show considerable biases in both SW- and LW-down fluxes as a result of a large and persistent underestimation in CF. Despite correcting known errors and performing updates to the system components, only minor differences in reanalyzed Arctic CF and surface radiative fluxes appear in R2 as compared with its predecessor R1 (Walsh et al. 2009). While the largest biases in 20CR appeared during the winter and early spring, it did perform better during the summer months over both stations as its monthly mean biases and RMSE's were considerably reduced. By comparing these results with those using earlier reanalyses in Walsh et al. (2009), the CFSR and ERA-Interim reanalyses illustrate an improvement in reanalyzed surface downwelling radiation fluxes.

While the main focus of this study was on the overall performance of several reanalysis datasets, further

investigation into the major causes of the biases in cloud and radiation fields should be considered. It was shown in this study that errors in reanalyzed CFs led to large errors in the surface radiation fluxes as compared with surface observations. However, while clouds do play a crucial role in the behavior of atmospheric radiation transport, other parameters, including cloud and aerosol properties, sea ice properties, land and ocean surface properties, and columnar loading of gases such as water vapor and ozone, can also have significant impacts on the surface radiation budget. Since clouds are known to vary in their effects on radiation transfer as a function of height, it would be useful to compare the reanalyzed fractional coverage of low, middle, and high clouds in each of the reanalyses. Investigating these parameters and their relationships to the earth's radiation balance may be a fundamental key in improving the radiation budgets contained in future reanalyses.

It is important to note that this evaluation focused only on reanalyzed CF and surface LW-down and SW-down fluxes over the Arctic region, and should not be considered an indication of the overall performance of each reanalysis. However, in a companion study over middle latitudes, Kennedy et al. (2011) also found that the CF and radiative fluxes derived from MERRA generally agreed better than those derived from the North American Regional Reanalysis (NARR) with ARM Southern Great Plains (SGP) ground-based observations. Furthermore, while utilizing two long-term surface-based observation stations does provide valuable information, these results may not be representative of the entire Arctic region, rather a localized representation. In a following study, we intend to extend these results by performing an Arctic-wide (70°–90°N) evaluation of these latest reanalyses using top of the atmosphere (TOA) radiative fluxes and CFs derived from Moderate Resolution Imaging Spectroradiometer (MODIS) and Clouds and the Earth's Radiant Energy System (CERES) observations. This will help fill in the gaps by providing further indication into specifically which regions in the Arctic contain the largest biases in radiative fluxes and in which reanalyses are these biases most pronounced.

While some of these reanalyses may be used as a baseline or reference for evaluating other datasets (climate models), this study will provide a quantitative uncertainty and identify the major biases contained in each reanalysis dataset. As numerous studies continue to be performed over various regions across the Arctic during different times of the year, these results may provide guidance into which reanalyses may be best suited for use in regards to the biases and accuracies in their reanalyzed variables. Furthermore, it is hoped that the findings of this study will offer insight into the areas of needed improvements with respect to the cloud and radiation parameterizations within future reanalyses.

Acknowledgments. MERRA was obtained from the Goddard Earth Sciences Data and Information Services Center, Greenbelt, Maryland, from their web site at http://disc.sci.gsfc.nasa.gov/mdisc. NCEP/DOE R2 and 20th Century Reanalysis V2 datasets were provided by the NOAA/OAR/ESRL PSD, Boulder, Colorado, from their web site at http://www.esrl.noaa.gov/psd/. CFSR data were obtained by the CISL Research Data Archive at NCAR in Boulder, Colorado, from their website at http://dss.ucar.edu/pub/cfsr.html, and ERA-I data were obtained from the ECMWF Data Server at http://data.ecmwf.int/data/. A special thanks to Dr. Ellsworth Dutton for BSRN observations at Barrow, Alaska; and Dr. Marion Maturilli for providing BSRN observations at Ny-Alesund, Norway. The University of North Dakota authors were supported by NASA NEWS project under Grant NNX07AW05G, the NASA CERES project under Grant NNX10AI05G, and NSF under Grant ATM0649549.

REFERENCES

Ackerman, T., and G. Stokes, 2003: The Atmospheric Radiation Measurement Program. *Phys. Today,* **56,** 38–45.

Berrisford, P., D. Dee, K. Fielding, M. Fuentes, P. Kallberg, S. Kobayashi, and S. Uppala, 2009: The ERA-Interim archive. ECMWF Tech. Rep. 1, 16 pp. [Available online at http://www.ecmwf.int/publications/library/do/references/show?id=89203.]

Bloom, S. C., L. L. Takacs, A. M. Da Silva, and D. Ledvina, 1996: Data assimilation using incremental analysis updates. *Mon. Wea. Rev.,* **124,** 1256–1271.

Bosilovich, M. G., J. Chen, F. R. Robertson, and R. F. Adler, 2008: Evaluation of global precipitation in reanalyses. *J. Appl. Meteor. Climatol.,* **47,** 2279–2299.

Bromwich, D. H., and S.-H. Wang, 2005: Evaluation of the NCEP–NCAR and ECMWF 15- and 40-yr reanalyses using rawinsonde data from two independent Arctic field experiments. *Mon. Wea. Rev.,* **133,** 3562–3578.

——, R. I. Cullather, and M. C. Serreze, 2000: Reanalyses depiction of the Arctic atmospheric moisture budget. *The Fresh Water Budget of the Arctic Ocean,* E. L. Lewis, Ed., Kluwer Academic Publishers, 163–196.

——, S.-H. Wang, and A. J. Monaghan, 2002: ERA-40 representation of the Arctic atmospheric moisture budget. *ECMWF Workshop on Reanalysis,* ECMWF Re-Analysis Project Report Series, Vol. 3, ECMWF, 287–298.

——, R. Fogt, K. I. Hodges, and J. E. Walsh, 2007: A tropospheric assessment of the ERA-40, NCEP, JRA-25 global reanalyses in the polar regions. *J. Geophys. Res.,* **112,** D10111, doi:10.1029/2006JD007859.

Chou, M.-D., 1992: A solar radiation model for use in climate studies. *J. Atmos. Sci.,* **49,** 762–772.

——, and K.-T. Lee, 1996: Parameterizations for the absorption of solar radiation by water vapor and ozone. *J. Atmos. Sci.,* **53,** 1203–1208.

——, and M. J. Suarez, 1999: A solar radiation parameterization for atmospheric studies. NASA Tech. Rep. Series on

Global Modeling and Data Assimilation 104606, Vol. 15, 40 pp.

——, ——, X. Z. Liang, and M. M.-H. Yan, 2001: A thermal infrared radiation parameterization for atmospheric studies. NASA Tech. Rep. Series on Global Modeling and Data Assimilation 104606, Vol. 19, 56 pp.

Clough, S. A., M. W. Shephard, E. J. Mlawer, J. S. Delamere, M. J. Iacono, K. Cady-Pereira, S. Boukabara, and P. D. Brown, 2005: Atmospheric radiative transfer modeling: A summary of the AER codes. *J. Quant. Spectrosc. Radiat. Transfer,* **91,** 233–244.

Compo, G. P., and Coauthors, 2006: Feasability of a 100-year reanalysis using only surface pressure data. *Bull. Amer. Meteor. Soc.,* **87,** 175–190.

——, and Coauthors, 2011: The twentieth century reanalysis project. *Quart. J. Roy. Meteor. Soc.,* **137,** 1–28.

Curry, J. A., J. Schramm, and E. E. Ebert, 1995: On the sea ice albedo climate feedback mechanism. *J. Climate,* **8,** 240–247.

Dee, D. P., and S. Uppala, 2009: Variational bias correction of satellite radiance data in the ERA-Interim reanalysis. *Quart. J. Roy. Meteor. Soc.,* **135,** 1830–1841.

Dong, X., and G. G. Mace, 2003: Arctic stratus cloud properties and radiative forcing derived from ground-based data collected at Barrow, Alaska. *J. Climate,* **16,** 445–461.

——, B. Xi, and P. Minnis, 2006: A climatology of midlatitude continental clouds from ARM SGP site. Part II: Cloud fraction and surface radiative forcing. *J. Climate,* **19,** 1765–1783.

——, ——, K. Crosby, C. N. Long, R. Stone, and M. Shupe, 2010: A 10-yr climatology of Arctic cloud fraction and radiative forcing at Barrow, Alaska. *J. Geophys. Res.,* **115,** D17212, doi:10.1029/2009JD013489.

Flynn, C., 2004: Vaisala ceilometer (Model CT25K) handbook. ARM Rep. TR-020, 17 pp.

Francis, J. A., 2002: Validation of reanalysis upper-level winds in the Arctic with independent rawinsonde data. *Geophys. Res. Lett.,* **29,** 1315.

——, E. Hunter, J. R. Key, and X. Wang, 2005: Clues to variability in Arctic minimum sea ice extent. *Geophys. Res. Lett.,* **32,** L21501, doi:10.1029/2005GL024376.

Hahn, C. J., S. G. Warren, and J. London, 1995: The effect of moonlight on observation of cloud cover at night, and application to cloud climatology. *J. Climate,* **8,** 1429–1446.

Hou, Y., S. Moorthi, and K. Compana, 2002: Parameterization of solar radiation transfer in the NCEP models. NCEP Office Note 441, 46 pp. [Available at http://www.emc.ncep.noaa.gov/officenotes/newernotes/on441.pdf.]

Iacono, M. J., E. J. Mlawer, S. A. Clough, and J. J. Morcrette, 2000: Impact of an improved longwave radiation model, RRTM, on the energy budget and thermodynamic properties of the NCAR Community Climate Model, CCM3. *J. Geophys. Res.,* **105,** 14 873–14 890.

Kalnay, E., and Coauthors, 1996: The NCEP/NCAR 40-Year Reanalysis Project. *Bull. Amer. Meteor. Soc.,* **77,** 437–471.

Kanamitsu, M., W. Ebisuzaki, J. Woollen, S. K. Yang, J. J. Hnilo, M. Fiorino, and G. L. Potter, 2002: NCEP-DOE AMIP-II Reanalysis (R-2). *Bull. Amer. Meteor. Soc.,* **83,** 1631–1643.

Kay, J. E., T. L'Ecuyer, A. Gettleman, G. Stephens, and C. O'Dell, 2008: The contribution of cloud and radiation anomalies to the 2007 Arctic sea ice extent minimum. *Geophys. Res. Lett.,* **35,** L08503, doi:10.1029/2008GL033451.

Kennedy, A. D., X. Dong, B. Xi, S. Xie, Y. Zhang, and J. Chen, 2011: A comparison of MERRA and NARR reanalysis datasets with the DOE ARM SGP continuous forcing data. *J. Climate,* **24,** 4541–4557.

Lanconelli, C., M. Busetto, E. G. Dutton, G. König-Langlo, M. Maturilli, R. Sieger, V. Vitale, and T. Yamanouchi, 2011: Polar baseline surface radiation measurements during the International Polar Year 2007-2009. *Earth Syst. Sci. Data,* **3,** 1–8.

Marty, C., and Coauthors, 2003: Downward longwave irradiance uncertainty under Arctic atmospheres: Measurements and modeling. *J. Geophys. Res.,* **108,** 4358, doi:10.1029/2002JD002937.

Mlawer, E. J., S. J. Taubman, P. D. Brown, M. J. Iacono, and S. A. Clough, 1997: Radiative transfer for inhomogeneous atmospheres: RRTM, a validated correlated-k model for the longwave. *J. Geophys. Res.,* **102,** 16 663–16 682.

Moorthi, S., H. L. Pan, and P. Caplan, 2001: Changes to the 2001 NCEP operational MRF/AVN global analysis/forecast system. *NWS Technical Procedures Bulletin,* Vol. 484, National Weather Service, Silver Spring, MD, 14 pp.

Ohmura, A., and Coauthors, 1998: Baseline Surface Radiation Network (BSRN/WCRP): New precision radiometery for climate change research. *Bull. Amer. Meteor. Soc.,* **79,** 2115–2136.

Onogi, K., and Coauthors, 2007: The JRA-25 Reanalysis. *J. Meteor. Soc. Japan,* **85,** 369–432.

Rayner, N. A., D. E. Parker, E. B. Horton, C. K. Folland, L. V. Alexander, D. P. Rowell, E. C. Kent, and A. Kaplan, 2003: Global analyses of sea surface temperature, sea ice, and night marine air temperature since the late nineteenth century. *J. Geophys. Res.,* **108,** 4407.

Rienecker, M. M., and Coauthors, 2008: The GEOS-5 Data Assimilation System—Documentation of versions 5.0.1, 5.1.0, and 5.2.0. NASA Tech. Rep. Series on Global Modeling and Data Assimilation 104606, Vol. 27, 92 pp.

Saha, S., and Coauthors, 2006: The NCEP Climate Forecast System. *J. Climate,* **19,** 3483–3517.

——, and Coauthors, 2010: The NCEP Climate Forecast System reanalysis. *Bull. Amer. Meteor. Soc.,* **91,** 1015–1057.

Serreze, M. C., and C. M. Hurst, 2000: Representation of mean Arctic precipitation from NCEP–NCAR and ERA reanalyses. *J. Climate,* **13,** 182–201.

——, and J. A. Francis, 2006: The Arctic amplification debate. *Climatic Change,* **76,** 241–264.

——, R. G. Barry, M. C. Rehder, and J. E. Walsh, 1995: Variability in atmospheric circulation and moisture flux over the Arctic. *Philos. Trans. Roy. Soc. London,* **352A,** 215–225.

Simmons, A., S. Uppala, D. Dee, and S. Kobayashi, 2007: ERA-Interim: New ECMWF reanalysis products from 1989 onwards. *ECMWF Newsletter,* No. 110, ECMWF, Reading, United Kingdom, 25–35.

Solomon, S., D. Qin, M. Manning, Z. Chen, M. Marquis, K. B. Averyt, M. Tignor, and H. L. Miller, 2007: Summary for policymakers. *Climate Change 2007: The Physical Science Basis,* S. Solomon et al., Eds., Cambridge University Press, 1–18.

Uppala, S. M., and Coauthors, 2005: The ERA-40 Re-Analysis. *Quart. J. Roy. Meteor. Soc.,* **131,** 2961–3012.

Walsh, J. E., W. L. Chapman, and D. H. Portis, 2009: Arctic cloud fraction and radiative fluxes in atmospheric reanalyses. *J. Climate,* **22,** 2316–2334.

Wendler, G., F. Eaton, and T. Ohtake, 1981: Multiple reflection effects on irradiance in the presence of arctic stratus clouds. *J. Geophys. Res.,* **86,** 2049–2057.

Whitaker, J. S., and T. M. Hamill, 2002: Ensemble data assimilation without perturbed observations. *Mon. Wea. Rev.,* **130,** 1913–1924.

Xu, K. M., and D. A. Randall, 1996: A semiempirical cloudiness parameterization for use in climate models. *J. Atmos. Sci.,* **53,** 3084–3102.